

DNA Intercalators

A Theoretical and Experimental Investigation of the Spectroscopic Properties of a DNA-Intercalator Salphen-Type Zn^{II} ComplexAlessandro Biancardi,^{*[a]} Azzurra Burgalassi,^[a] Alessio Terenzi,^[b] Angelo Spinello,^[b] Giampaolo Barone,^[b] Tarita Biver,^{*[a]} and Benedetta Mennucci^[a]

Abstract: The photophysical and DNA-binding properties of the cationic zinc(II) complex of 5-triethylammonium methyl salicylidene *ortho*-phenylenediiminato (ZnL²⁺) were investigated by a combination of experimental and theoretical methods. DFT calculations were performed on both the ground and the first excited states of ZnL²⁺ and on its possible mono- and dioxidation products, both in vacuo and in selected solvents mimicked by the polarizable continuum model. Comparison of the calculated absorption and fluorescence transitions with the corresponding experimental data led to the conclusion that visible light induces a two-electron photooxidation process located on the phenylenediiminato ligand. Kinetic measurements, performed by monitoring absorbance changes over time in several solvents, are in agreement with a slow unimolecular photooxidation process, which is faster in water and slower in less polar solvents. Moreover, structural details of ZnL–DNA binding were

obtained by DFT calculations on the intercalation complexes between ZnL and the d(ApT)₂ and d(GpC)₂ dinucleoside monophosphate duplexes. Two main complementary binding interactions are proposed: 1) intercalation of the central phenyl ring of the ligand between the stacked DNA base pairs; 2) external electrostatic attraction between the negatively charged phosphate groups and the two cationic triethylammonium groups of the Schiff-base ligand. Such suggestions are supported by fluorescence titrations performed on the ZnL/DNA system at different ionic strengths and temperatures. In particular, the values of the DNA-binding constants obtained at different temperatures provided the enthalpic and entropic contributions to the binding and confirmed that two competitive mechanisms, namely, intercalation and external interaction, are involved. The two mechanisms are coexistent at room temperature under physiological conditions.

Introduction

Salphen and salen^[1] are among the oldest and most popular ligands in coordination chemistry. The zinc(II) ion is essential in most biological systems, since it is present in a plethora of enzymes with structural (influencing both stability and conformation) and catalytic functions.^[2] Zinc complexes are of current interest for their applications in molecular sensors,^[3] as emissive materials in organic light-emitting diodes,^[4] in homogeneous catalysis,^[5] as building blocks for supramolecular chemistry,^[6] and for their potential medical applications.^[7] They are also relevant as model systems to better understand the structure and the functions of zinc enzymes^[2] and zinc-enzyme inhibition.^[8] Several studies on other salen-type metal complexes

have been also reported in the literature,^[9] including their interaction with DNA.^[7,10–12] The interest in DNA binding by transition metal complexes is due to the potential discovery of novel metallodrugs.^[13] For example, it is well known that DNA is the target of the most common clinically used platinum-based drugs.^[14]

Recently, the cationic ligand 5-triethylammonium methyl salicylidene *ortho*-phenylenediiminato has been used to prepare first-row transition metal complexes with improved water solubility and DNA-binding affinity.^[12,15] UV/Vis absorption, circular dichroism,^[12] and linear dichroism^[16] measurements indicate that the zinc(II) complex of this Schiff-base ligand (ZnL²⁺, see Figure 1) tightly binds DNA by intercalation. However, other aspects remain to be investigated, such as the role of the positive charge on the side-chain arms of the Schiff-base ligand. Moreover, ZnL²⁺ shows marked enhancement of the fluores-

[a] A. Biancardi, Dr. A. Burgalassi, Dr. T. Biver, Prof. B. Mennucci
Dipartimento di Chimica e Chimica Industriale
Università di Pisa, Via Risorgimento 35, 56126 Pisa (Italy)
E-mail: alessandro.biancardi@for.unipi.it
tarita.biver@unipi.it

[b] Dr. A. Terenzi, Dr. A. Spinello, Dr. G. Barone
Dipartimento di Scienze e Tecnologie Biologiche
Chimiche e Farmaceutiche, Università di Palermo
Viale delle Scienze, Parco d'Orleans II
Edificio 17, 90128 Palermo (Italy)

Supporting information for this article is available on the WWW under
<http://dx.doi.org/10.1002/chem.201304876>.

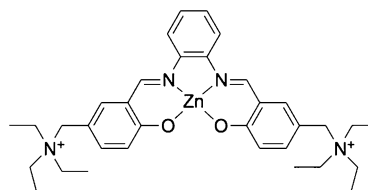


Figure 1. Molecular structure of ZnL²⁺.

cence intensity when its aqueous solutions are exposed to the visible light from a tungsten source; interestingly, this is inhibited when the complex is intercalated into native calf thymus (ct) DNA.^[10] By studying frozen solutions of a Zn^{II} salphen complex in organic solvents at 77 K, Germain et al.^[17] first recognized that 5 min exposure to visible light causes a photoinduced oxidation process giving rise to an EPR signal corresponding to the formation of an $S=1/2$ radical.

The effect of light on complexes of d-block metals and the subsequent effects on biomolecules like DNA is well-documented, for instance, as concerns photodynamic therapy.^[18] Metal compounds, such as ruthenium and osmium complexes, were found to undergo a molecular light-switch effect that is promising for selective sequence sensing.^[19] The light-switching mechanism was also successfully investigated from the theoretical point of view.^[20,21]

To clarify the photophysical properties of ZnL²⁺, we performed a quantum-mechanical (QM) study of its absorbance and fluorescence emission in environments of increasing complexity and in its singlet, doublet, triplet, and mono- and dioxidized forms. First we considered homogeneous solutions by simulating their effects in terms of a polarizable continuum model (PCM),^[22] introduced the model photooxidation effects, and finally analyzed intercalation into double-stranded DNA. Detailed computational simulations of the intercalated structures were aimed at an in-depth understanding of their photophysical characteristics, which is still lacking. In particular, the effects of different environments/binding modes on the absorption and fluorescence of these complexes have never been considered in detail by using computational tools. However, accurate QM modeling (coupled with both atomistic and continuum descriptions of the environment) of the absorption and fluorescence properties of the intercalated probe is of great help for understanding the microscopic details of the interaction between small molecules and nucleic acids, and it may be an important tool for the analysis of processes of biochemical and biophysical significance, together with providing a structural framework for new hypotheses.^[23]

Results and Discussion

Gas phase and aqueous solution

To understand the important changes in the photophysical behavior of ZnL²⁺ under different environmental conditions, we first analyzed the geometrical structures of both ground and excited states of the isolated and solvated system using a (TD)DFT approach combined with a PCM description of the aqueous solvent. The ZnL²⁺ complex (Figure 1) is positively charged and has several rotational degrees of freedom (the main ones are shown in Figure S1 of the Supporting Information).

The optimized ground- and excited-state structures (Figure S2 of the Supporting Information) indicate that the excitation process involves planarization of the system (see also Table S1 of the Supporting Information). To obtain a more refined description of solvation in water, we also analyzed the ef-

fects of the interaction with one or two explicit water molecules coordinating to the zinc ion to give the pentacoordinate complex [ZnL(H₂O)]²⁺ and/or interacting with the phenoxyl oxygen atoms. In the former case the explicit water molecule forms two hydrogen bonds with the hydroxyl groups, whereas in the latter case the second explicit water molecule is coordinated to the metal center (see Figure S3 of the Supporting Information). To include also the effects of outer solvent shells, the clusters were embedded in a PCM solvent.

Figure 2 compares the experimental spectrum of the complex in water and the calculated spectra of the complex in vacuo and in water. The visible absorption spectrum of ZnL²⁺

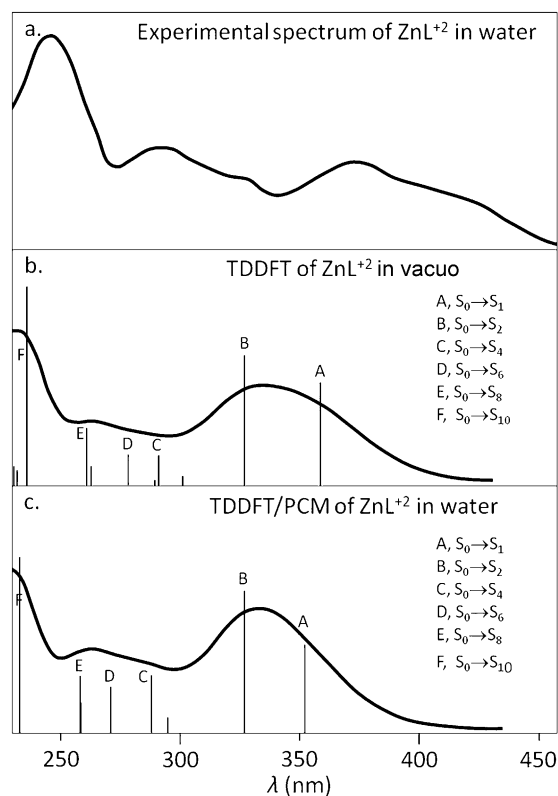


Figure 2. Comparison between the experimental absorption spectrum of ZnL²⁺ in buffered aqueous solution (a) and the calculated TD-DFT absorption spectra in vacuo (b) and in water (c) by using PCM.

in aqueous solution is mainly determined by a large absorption band at about 397 nm, which is attributed to a metal-perturbed intraligand electronic transition. This band is common to both the free and bound ligand (see Figure S4 of the Supporting Information). The UV absorption spectrum is composed of strong bands in which the zinc atom has an effect. As shown in Figure 2, the calculated absorption bands are systematically blueshifted compared with the experimental ones. The calculated spectrum seems to be less affected by this shift on moving from the visible to the UV region. Figure 2 shows good agreement between experimental and calculated spectra, especially when solvent effects are included. In particular, inclusion of the solvent mainly modifies the relative transition intensities. The spectrum of the free ligand (Figure S4 of the

Supporting Information) shows that the zinc only has a shifting effect on the first two transitions, but it has a key effect on the part of the spectrum below 300 nm.

The most important transitions in the spectra were analyzed by the natural transition orbitals (NTO) method.^[24] This is a compact orbital representation of the electronic-transition density matrix, mainly in term of a few single hole/particle NTO pairs.^[25] The dominant NTO pairs are shown in Figure 3.

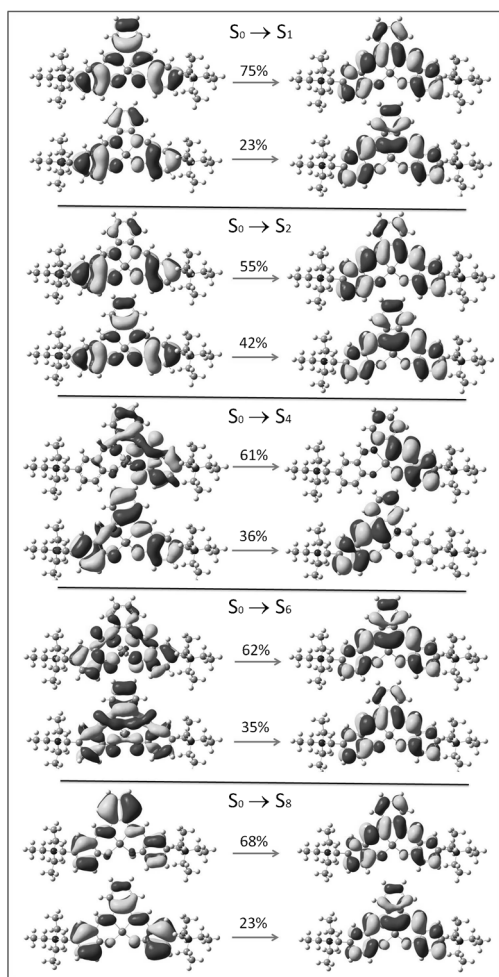


Figure 3. Dominant NTO pairs for the most important transitions of ZnL^{2+} in vacuo (shown in Figure 2b). The NTO transition amplitudes are also shown.

The NTO analysis showed that the first two transitions are mainly located on the ligand (Figure 3) and, as a result, this band is practically the same for the free (Figure S4 of the Supporting Information) and bound ligand (Figure 2b, c). On the other hand, the presence of the zinc ion becomes more important for transitions at wavelengths lower than 300 nm, as shown in Figure 3 for the NTOs related to the $S_0 \rightarrow S_4$ and $S_0 \rightarrow S_6$ transitions.

Table 1 compares the experimental and calculated absorption and emission energies and Stokes shifts of ZnL^{2+} in water. The calculated absorption energies refer to the $S_0 \rightarrow S_2$ transition, whereas the emission energy refers to the transition from the lowest excited state. Inclusion of the solvent by using

Table 1. Comparison between experimental and calculated absorption (ABS) energies, emission (FLU) energies, and Stokes shifts (SS) of ZnL^{2+} . The calculated TDDFT/PCM + 1 water or + 2 water data refer to ZnL^{2+} plus one and two explicit water molecules in a PCM solvent, as shown in Figure S3 of the Supporting Information. All values are in electron volts.

| Method | ABS | FLU | SS |
|---------------------|------|------|------|
| exptl | 3.36 | 2.58 | 0.78 |
| in vacuo | 3.80 | 2.66 | 1.14 |
| TDDFT/PCM | 3.80 | 2.75 | 1.05 |
| TDDFT/PCM + 1 water | 3.84 | 2.77 | 1.07 |
| TDDFT/PCM + 2 water | 3.85 | 2.66 | 1.19 |

a PCM description has negligible effects on the absorption energies, but it modifies the emission energies by inducing a blueshift of 0.09 eV. The inclusion of one or two explicit water molecules only slightly affects the absorption spectra, whereas a redshift is observed for the emission in the complex with a zinc-coordinated water ligand.

The photooxidation process

Recent studies indicate that exposure to a tungsten lamp causes oxidation of ZnL^{2+} in aqueous solution, whereas this process is inhibited when the metal complex is intercalated in DNA.^[10,17] To clarify such behavior, we performed a QM/PCM study considering the mono-oxidized (ZnL^{3+} , doublet) and di-oxidized (ZnL^{4+} , singlet and triplet) forms of ZnL^{2+} (see Table S2 of the Supporting Information for a list of the main geometrical parameters). The calculations showed that the oxidation is mainly located on the aromatic rings of the ligand (Figure S5 of the Supporting Information). Comparison between experiment and calculation (Figure 4 and Figure S6 of the Supporting Information) seems to show that the experimental spectrum of the oxidized complex corresponds to the dioxidized triplet radical $\text{ZnL}^{4+}(\text{T})$. This is also confirmed by the relative energies calculated in water, which showed that $\text{ZnL}^{4+}(\text{T})$ is about 9 kcal mol⁻¹ more stable than $\text{ZnL}^{4+}(\text{S})$.

The kinetics of the photooxidation process of ZnL^{2+} was experimentally monitored by measuring the change in absorbance in time at different wavelengths (245, 293, and 373 nm). The monoexponential trends obtained (Figure S7A of the Supporting Information) were interpolated to obtain the time constant $1/\tau$, which was found to be independent of the ZnL^{2+} concentration (Figure S7B of the Supporting Information), in agreement with a unimolecular reaction. The data show that the kinetics of the process depend on the solvent, as shown in Figure 5. In particular, the process is faster in water and the rate monotonously decreases with decreasing solvent polarity. On the other hand, for solvents of similar polarities (THF and 1,4-dioxane), the time constants are similar.

This behavior is difficult to simulate by calculations, as the oxidation process of ZnL^{2+} is more likely driven by an excited-state electron transfer, as shown by Germain et al.^[17] However, in the approximation of considering the solvent dependence of the oxidation process to be similar in the ground and excited states, calculated vertical ionization energies [$\text{ZnL}^{+2} > \text{ZnL}^{+}$

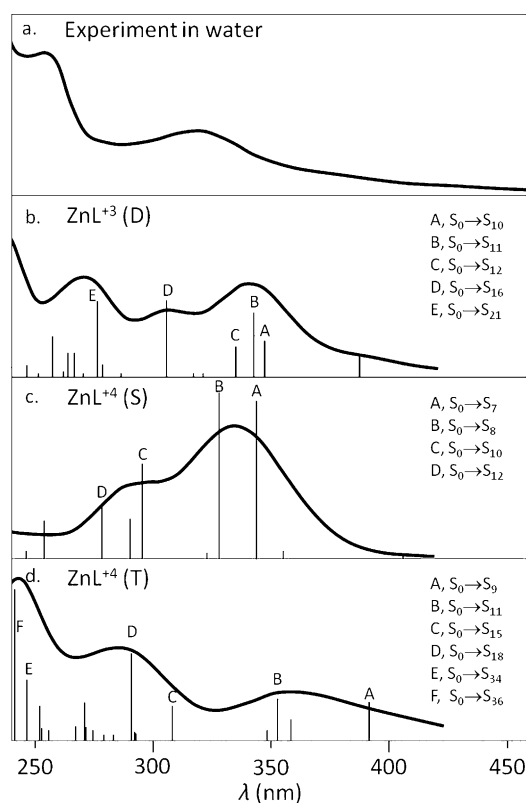


Figure 4. Comparison between calculated (b–d) absorption spectra of ZnL^{3+} (D spin state) and ZnL^{4+} (S and T spin states) in water (PCM) and the experimental spectra of light-exposed species in water (a).

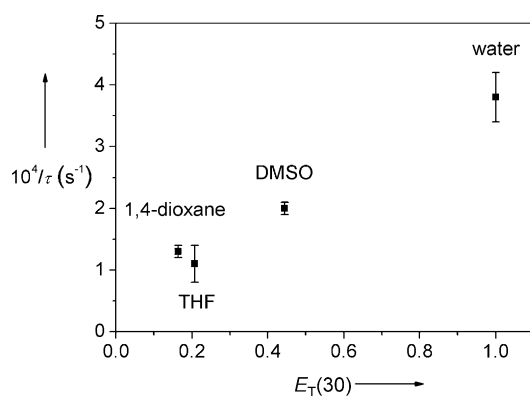


Figure 5. Dependence of the reciprocal time constant $1/\tau$ for ZnL^{2+} photo-oxidation on the solvent polarity ($E_{\text{T}}(30)$ scale^[50]), $T = 25^\circ\text{C}$.

$^4(\text{T})$] decrease on increasing the polarity of the solvent, from 11.9 eV in the gas phase to 7.0 eV in THF to 6.3 eV in water, in agreement with the experimental plot in Figure 5.

DNA intercalation

Since no experimental intercalated structures are available for ZnL^{2+} , we obtained two possible pockets of the intercalated system in alternating AT and GC dodecanucleotides from MD simulations by following a recently reported procedure.^[26] The

root mean square deviation (RMSD) for all non-hydrogen atoms is shown in Figure S8 of the Supporting Information, which shows that the initial structure of both intercalation complexes suddenly changes after about 1 ns, by about 3 Å in the RMSD. Then, oscillations of about 2 Å of RMSD occur around the equilibrium geometry, largely involving the tails of the two dodecanucleotides and much less the structure of the metal complex and the four stacked DNA bases of the intercalation pocket. In particular, the metal complex remains tightly intercalated between the fifth and sixth bases for the whole simulation time. The equilibrium geometry was used as starting point for further geometry optimizations by hybrid two-layer QM/molecular mechanics (MM) calculations with DFT as QM method and the Amber99 force field as MM method.^[26] Because of the large size of the systems, here we modeled the double-stranded DNA pockets using the $\text{d}(\text{ApT})_2$ and $\text{d}(\text{GpC})_2$ simplified models, which limit the interaction between ZnL^{2+} and the DNA to the first neighborhoods. As shown previously,^[23] inclusion of at least the effects of the lateral sugar/phosphate chains in addition to the stacking bases is crucial to obtain a reliable description of the short-range interactions between the DNA-bound molecule and the pocket; the selected model systems are shown in Figure 6.

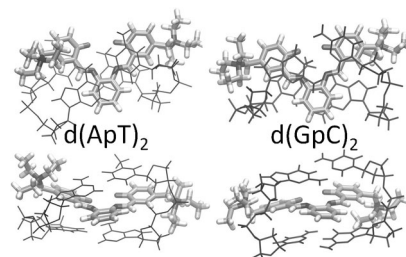


Figure 6. Optimized molecular structures of ZnL^{2+} intercalated in $\text{d}(\text{GpC})_2$ (left) and $\text{d}(\text{ApT})_2$ (right).

A straightforward method for the calculation of the transition energies relies on a fully QM strategy for both ZnL^{2+} and the intercalation pocket. An alternative approach is based on the use of a hybrid QM/polarizable MM (QM/MMpol)^[27] method describing the DNA pocket with a polarizable classical force field given by point charges and induced dipoles. The comparison between the fully QM and the QM/MMpol method is useful in disentangling the different effects of the DNA pocket. The solvent can be taken into account at the PCM level by using a QM/PCM or a QM/MMpol/PCM^[28] approach. The optimized ground-state structures of ZnL^{2+} intercalated in $\text{d}(\text{ApT})_2$ and $\text{d}(\text{GpC})_2$ are shown in Figure 6. Important optimized dihedral angles are reported in Table S1 of the Supporting Information.

Figure 7 compares the experimental and calculated absorption spectra of ZnL^{2+} intercalated in the $\text{d}(\text{GpC})_2$ and $\text{d}(\text{ApT})_2$ pockets. This comparison shows that intercalation causes significant changes in the absorption spectrum. Since we performed a fully QM study on both ZnL^{2+} and the DNA pocket, our calculated spectra explicitly describe the effects of the QM

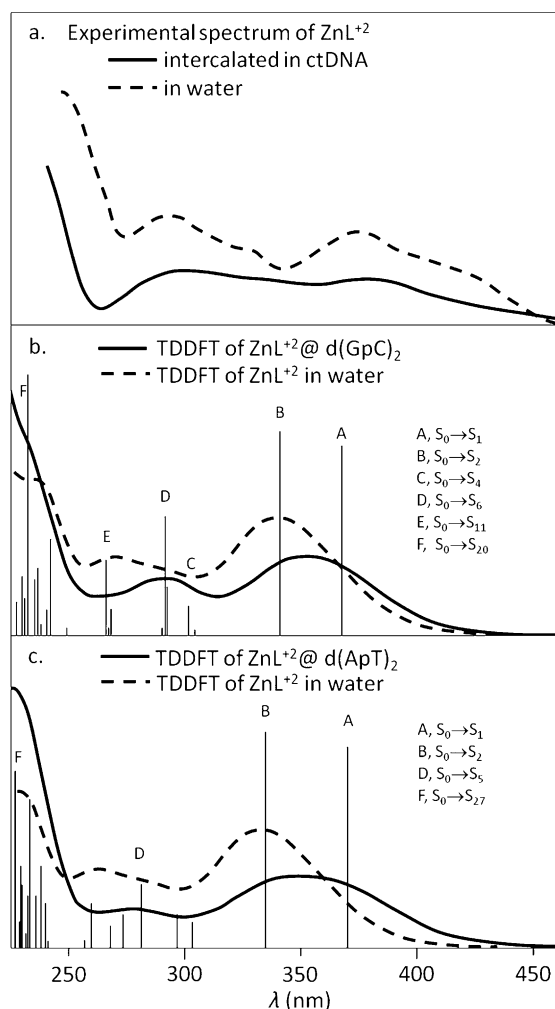


Figure 7. Comparison between the experimental absorption spectrum of ZnL^{2+} intercalated in ctDNA (a) and those calculated in water (PCM) for ZnL^{2+} intercalated in $\text{d}(\text{GpC})_2$ (b) and $\text{d}(\text{ApT})_2$ (c). The corresponding spectra of free ZnL^{2+} are also shown for each case (dashed lines). For the experimental spectrum of the ZnL^{2+} /DNA complexes (25°C), low ionic strength ($1 \times 10^{-3}\text{ M}$ buffer) and excess polymer ($C_D = 54\ \mu\text{M}$, $C_P/C_D = 10$) were used to ensure quantitative dye reaction; in the shown spectrum, the DNA contribution to absorbance was subtracted.

intercalation pocket. This is crucial for modeling the spectrum at wavelengths longer than 300 nm, which is characterized by strong mixing between ZnL^{2+} and the DNA pocket. Good qualitative agreement is found between the calculated and the experimental spectra (Figure 7). In particular, intercalation would cause a decrease of the intensity of the dye bands and their shift to higher wavelengths, which is fully reproduced in the calculated spectra. The inclusion of the solvent by using a continuum PCM causes only a slight modification of the spectra.

Table 2 lists the experimental and calculated absorption and emission energies of intercalated ZnL^{2+} . As for the isolated complex, the calculated absorption energies refer to the $S_0 \rightarrow S_2$ transition, whereas the emission energies refer to transition from the lowest excited state.

The most important transitions in the spectra were analyzed by the NTO method (see Figure 8 and Figure S7 of the Sup-

Table 2. Comparison between experimental and calculated absorption (ABS), emission (FLU) energies, and Stokes shifts (SS) for different ZnL^{2+} /polynucleotide systems. All values are in electron volts. The comparison with the available experimental data in ctDNA is performed by averaging the results calculated for $\text{d}(\text{ApT})_2$ and $\text{d}(\text{GpC})_2$, considering that ctDNA is constituted by 60% AT and 40% GC base pairs, and assuming an equal intercalation affinity.

| Dinucleotide | Method | ABS | FLU | SS |
|--------------------------|----------------|------|------|------|
| $\text{d}(\text{ApT})_2$ | QM/QM | 3.73 | 2.59 | 1.14 |
| | QM/QM/PCM | 3.70 | 2.65 | 1.05 |
| | QM/MMpol/PCM | 3.77 | 2.75 | 1.02 |
| $\text{d}(\text{GpC})_2$ | QM/QM | 3.64 | 2.42 | 1.22 |
| | QM/QM/PCM | 3.64 | 2.48 | 1.16 |
| | QM/MMpol/PCM | 3.73 | 2.53 | 1.20 |
| ctDNA | exptl | 3.24 | 2.53 | 0.71 |
| | (QM/QM) | 3.69 | 2.52 | 1.17 |
| | (QM/QM/PCM) | 3.68 | 2.58 | 1.09 |
| | (QM/MMpol/PCM) | 3.75 | 2.66 | 1.09 |

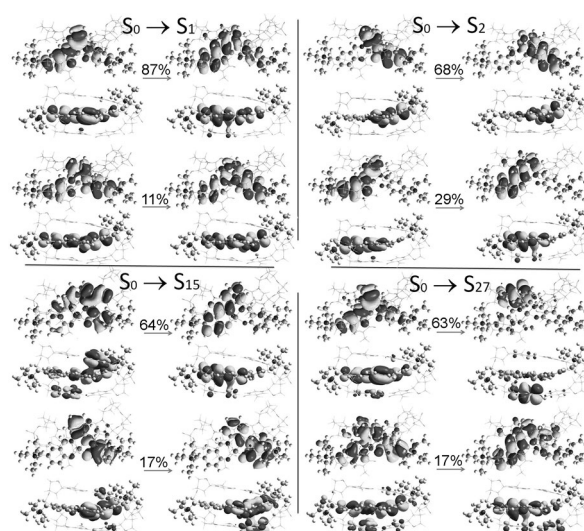


Figure 8. Dominant NTOs pairs for the most important transitions of ZnL^{2+} bound to $\text{d}(\text{ApT})_2$ (see Figure 7e). The NTO transition amplitudes are also shown.

porting Information for AT and GC, respectively). This analysis shows that all transitions (even those at lower energies) are characterized by non-negligible charge-transfer contributions between the base pairs and the DNA. The relevance of this mixing in a different intercalated molecule was previously suggested.^[21,29] The comparison between the isodensity surfaces of free and DNA-bound ZnL^{2+} shows that the intercalation leads to breaking of the symmetry of the virtual orbitals (see Figure 3, Figure 8, and Figure S9 of the Supporting Information). Analysis of the orbitals involved in the different transitions showed that the first two excitations are mainly located on the ligand, whereas higher-energy transitions also involve increasing contributions from both the zinc atom and the adjacent bases.

The binding was further analyzed by performing spectrofluorometric titrations to determine the variation in fluorescence of the system on addition of different amounts of DNA.

The interaction between ZnL^{2+} and natural DNA was represented by an apparent reaction [Eq. (1)]



where D and PD denote the free and bound ZnL^{2+} complex respectively, and P indicates a free site on the DNA polymer. In agreement with previous findings,^[10] the ZnL^{2+} /DNA solutions are stable to light.

One example of the obtained binding isotherms ($\Delta F = F - f_D C_D$, where $f_D = F^\circ / C_D$ and F° is the fluorescence measured in the absence of DNA) is shown in Figure S10A of the Supporting Information. The data were analyzed according to Equation (2) by using a procedure that first disregards the $\Delta F / \Delta f^2$ term ($\Delta f = f_{PD} - f_D$ is the amplitude of the isotherm) and then calculates it iteratively.^[30]

$$C_P C_D / \Delta F + \Delta F / \Delta f^2 = (C_P + C_D) / \Delta f + 1 / K \Delta f \quad (2)$$

At convergence, the value of the equilibrium constant K for Equation (1) is calculated by the slope/intercept ratio of the straight line interpolating data points in the $(C_P C_D / \Delta F + \Delta F / \Delta f^2)$ versus $(C_P + C_D)$ plot (Figure S10B of the Supporting Information). At 25 °C and an ionic strength of 0.11 M, $K = (3.5 \pm 0.2) \times 10^4 \text{ M}^{-1}$, in agreement with previous UV/Vis estimations.^[12]

The experiments were repeated under different conditions of added salt (NaCl content) or temperature. Figure 9A is a double-logarithmic plot showing the dependence of K on the salt content of the medium. According to Record et al.^[31] the slope of the plot corresponds to $0.88m$, where m is the number of sodium ions displaced from the DNA double helix due to the binding of one charged interacting molecule. It turns out that $m = 0.7 \pm 0.1$. This value is significantly lower than the +2 total charge borne by ZnL^{2+} , and lower than the values obtained for other DNA-intercalating metal complexes.^[32] However, in the herein-analyzed system, the positive charge is located quite far away from the central aromatic (i.e., intercalating) moiety. This result suggests that the protruding lateral residues only partially participate in the binding.

Figure 9B shows the binding constants obtained by varying the temperature between 5 and 45 °C. These data display a biphasic trend. Possible complex bleaching was carefully checked and ruled out; the fluorescence characteristics of the systems remained unchanged in the whole analyzed temperature range. Therefore, this behavior should be ascribed to the presence of a complex binding mechanism, in which at least two binding modes coexist. From the slope ($-\Delta H/R$) and intercept ($\Delta S/R$) of the two linear trends shown in Figure 9B, the values of the enthalpy and entropy variations (ΔH and ΔS , respectively) of the two limiting binding modes can be obtained. These data are collected in Table S3 of the Supporting Information. According to Chaires,^[33] the values of ΔH and ΔS provide information on the binding mode of a small molecule to a polynucleotide. The data at $T > 25^\circ\text{C}$ (highly negative ΔH , negative ΔS) are in agreement with intercalation; on the other hand, for $T \leq 25^\circ\text{C}$, the small positive ΔH and positive ΔS reveal the

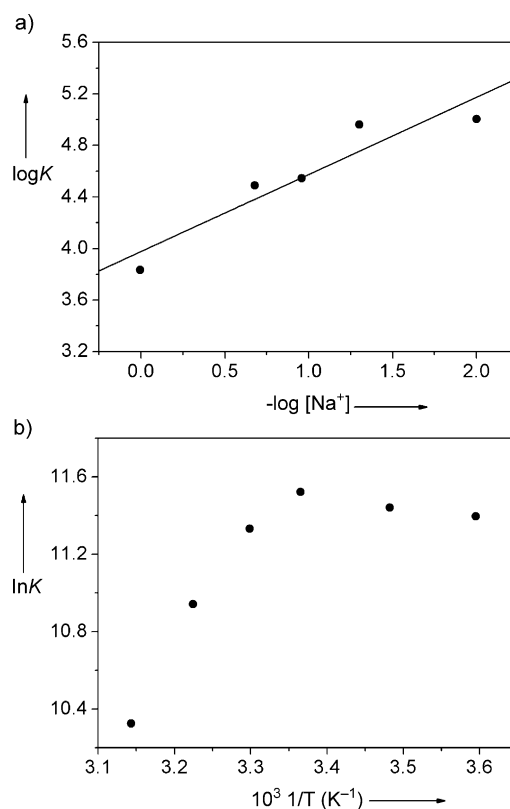


Figure 9. Dependence of the binding constant for the ZnL^{2+} /DNA system on salt content (a) and temperature (b). pH 7 (sodium cacodylate (NaCac buffer), $T = 25^\circ\text{C}$ (a), $I = 0.01 \text{ M}$ (NaCac) (b).

presence of a binding mode with external features. On the whole, the data suggest a complex binding mode in which both features play a role. Other bifunctional intercalating molecules with positively charged pendant arms were also found to exhibit complex binding modes in which the prevalence of external binding or intercalation depends on experimental conditions such as dye loading.^[34]

Conclusion

The kinetics of the photochemical reaction that occurs for the cationic Schiff-base zinc(II) complex ZnL^{2+} on exposure to visible light from a tungsten lamp involves a unimolecular process. This is faster in water and slows down in less polar solvents. The process was interpreted by comparison of the experimental and calculated absorption/fluorescence spectra to involve a two-electron photooxidation of the coordinated Schiff-base ligand of ZnL^{2+} to give the triplet radical $\text{ZnL}^{4+}(\text{T})$.

The calculated spectra of ZnL^{2+} intercalated in both $d(\text{ApT})_2$ and $d(\text{GpC})_2$ correctly reproduce the hypochromic effect experimentally observed for ZnL^{2+} intercalated in natural DNA. The intraligand band of the zinc(II) complex, which consists of two transitions to the first and second excited electronic states, is redshifted by about 0.12 eV on going from the free system (in water) to the intercalated system, and the calculations gave 0.11 eV when the shift is averaged over the two pockets.

The values of the experimental DNA-binding constants obtained at different temperatures provided the enthalpic and entropic contributions to the DNA binding and showed that two interaction mechanisms are involved (intercalation and external interaction at high and low temperature, respectively) and that the two mechanisms coexist at room temperature under physiological conditions. Remarkably, this result is supported by the analysis of the structures of the intercalation complexes, optimized by DFT. In fact, the latter are characterized by two main complementary binding interactions: 1) intercalation in the stacked AT–AT or GC–GC base pairs; 2) external electrostatic interaction between the negatively charged phosphate groups and the triethylammonium cationic groups of the Schiff-base ligand.

There is great interest in compounds that can interact with light in a particular way, for instance in the framework of selective light-switch sensors for biomolecules. However, in-depth mechanistic studies dealing with these systems are less abundant. The salen and salphen ligands have been known for a long time, but the possible photoinduced oxidation of their metal complexes had not been elucidated. In this work the combined use of experiments and theoretical calculations at the (TD)DFT level of QM theory provided important information both on the process of the metal complex oxidation and on its interaction with DNA. This approach is not only interesting for this particular system, but constitutes a promising tool to be used in similar studies.

Experimental Section

Computational details

The molecular systems investigated in the calculations were 1) ZnL^{2+} and its oxidized derivatives in the gas phase and in water; 2) ZnL^{2+} intercalated in a GC or AT double-stranded DNA pocket. The ground- and excited-state geometry optimizations and the absorption and emission calculations were performed at the (TD)DFT level of QM theory by using the M05-2X functional^[35] and the 6-311+G(d,p) basis set. This functional was chosen for its ability to describe both noncovalent interactions^[36] and zinc complexes.^[37] Open-shell DFT/TDDFT calculations for triplet and doublet states were carried out by using the unrestricted self-consistent field formalism. All the calculated absorption spectra were produced by convolution of the vertical transitions energies by using Gaussian functions of fixed full width at half-maximum of 0.24 eV. All the geometry optimizations were performed without imposing any constraints, whereas, in the case of the intercalated systems, the DNA pocket structures were kept frozen and described by using the smaller 6-31G basis set, analogously to previous works.^[23] The integral equation formalism^[38] version of the polarizable continuum model (PCM)^[22] was used to describe the effects of the solvent both on the ground and the excited states. PCM cavities were built up as a series of interlocking spheres centered on atoms with the UFF radii. The intercalation pockets were obtained as described in ref. [26] by combining a molecular dynamics (MD) simulation with a following ONIOM calculation. The MD simulations were conducted for 20 ns by using the Gromacs 4.5.3 software package^[39] on $[\text{ZnL}]/[\text{dodeca(dA-dT)}]_2$ and $[\text{ZnL}]/[\text{dodeca(dG-dC)}]_2$ intercalated complexes in the presence of explicit TIP3P water molecules with the Amber99 force field^[40] with Parmbsc0 nucleic acid torsions.^[41]

The relaxed geometries were optimized by two-layer ONIOM calculations,^[42] with the aim of performing a high-level calculation on the intercalation pocket and to take account of the constraining effects of the double-helical structure at lower levels of theory. The MPWB1K DFT functional and the dzvp basis set were used in the higher layer to suitably model the hydrogen bonding and π – π stacking interactions between the sixth and seventh Watson–Crick base pairs. The Amber99 force field was used in the lower layer of the ONIOM calculations.

To evaluate the importance of a QM description of the intercalation pockets constituted by the d(ApT)_2 and d(GpC)_2 dinucleoside monophosphate duplexes in the determination of absorption and fluorescence energies of ZnL^{2+} , two models were compared. In the first model, denoted QM/QM/PCM, a full QM description was used for both the complex and the DNA fragments constituting the pockets. As in the geometry optimizations, the DNA fragments were described with a smaller basis set (6-31G). The second model, denoted QM/MMPol/PCM,^[28] instead used a QM description only for ZnL^{2+} , whereas the pockets were described with fixed charges and induced dipoles. The fixed charges were obtained from a fit of the electrostatic potential of fragment by using the Merz and Kollman method^[43] with the same functional and the same basis set as used in the QM calculations. The induced dipoles were obtained in terms of isotropic polarizabilities placed on each MM atom. We adopted the Thole model, which avoids problems of intramolecular overpolarization by using a smeared dipole–dipole interaction tensor.^[44] Atomic isotropic polarizability values were taken from the fit of experimental molecular polarizabilities performed by van Duijnen and Swart by using the linear version of Thole dipole–dipole tensor.^[45] In both the QM/QM and QM/MMPol descriptions, the effects of the rest of the DNA and of the solvent were simulated by using a PCM description. In the case of QM/MMPol/PCM, the two classical parts (MMPol and PCM) were allowed to mutually polarize. The vertical ionization potential (VIP) was evaluated as the difference between the energy of the optimized structure before ionization and that of the ionized system at the same geometry.^[46] To effectively model the solvent effect, it is necessary to use the non-equilibrium version of the PCM. In fact, the ionization process can be seen as a vertical process in which the fast change in the molecular charge density is coupled with a fast (mainly electronic) and a slow (mainly orientational) response of the solvent molecules, similar to the cases of electronic excitation and electron transfer. All calculations were performed with the Gaussian 09 package.^[47]

Materials

The zinc(II) complex was synthesized by a recently reported procedure,^[10,15,16] by mixing 5-(triethylammoniummethyl) salicylaldehyde chloride, 1,2 phenylenediamine, and zinc(II) perchlorate in a 2:1.1:1 molar ratio. A basic solution (NaOH) of salicylaldehyde in EtOH/H₂O was added dropwise to a previously prepared ethanolic solution of the diamine and the metal perchlorate. The 5-(triethylammoniummethyl) salicylaldehyde chloride ligand was prepared from 5-chloromethyl salicylaldehyde and triethylamine in THF.^[12] The product was characterized by ¹H NMR spectroscopy.^[16]

Stock solutions of ZnL^{2+} (perchlorate salt, $M = 807.075 \text{ g mol}^{-1}$) were prepared by dissolving weighed amounts of the solid in MilliQ ultrapure water and kept in the dark at -20°C . Working solutions were obtained by dilution of the stocks, kept in the dark at 4°C , and used within 2 d. ZnL^{2+} concentration was also checked spectrophotometrically ($\epsilon_{373} = 1.52 \times 10^4 \text{ M}^{-1} \text{ cm}^{-1}$ ^[12]). Solutions in nonaqueous solvents were prepared by dissolving weighed

amounts of the solid, kept in the dark at 4 °C, and used within 2 d. The molar concentration of the dye is denoted C_D .

DNA (from calf thymus, lyophilized sodium salt, highly polymerized) was purchased from Sigma and its length was reduced to about 700 base pairs by using a sonication procedure described elsewhere.^[48] Stock solutions of the polynucleotides were standardized spectrophotometrically ($\epsilon = 13200 \text{ M}^{-1} \text{ cm}^{-1}$ at 260 nm).^[49] The polynucleotide concentration was expressed in molarity of base pairs and denoted C_p . All solutions were prepared with Millipore ultrapure water, which was also used as the reaction medium. In the case of the DNA measurements, small amounts of sodium cacodylate (Fluka, $(\text{CH}_3)_2\text{AsO}_2\text{Na}$, $1.0 \times 10^{-2} \text{ M}$) buffer were added to the working solutions to keep the pH constant at 7.0. The nonaqueous solvents THF (purity $\geq 99.8\%$, dried by distillation over potassium) and 1,4-dioxane (spectrophotometric grade, purity 99%) were from Sigma-Aldrich, whereas DMSO (purity $\geq 99.5\%$) was from Carlo Erba. All other chemicals were of analytical grade from Sigma and were used without further purification.

Experimental methods

Measurements of pH were made with a Metrohm 713 pH meter equipped with a combined glass electrode. Spectrophotometric measurements were performed on a PerkinElmer Lambda 35 spectrophotometer. Fluorescence measurements were carried out on a PerkinElmer LS55 spectrofluorometer. Both apparatuses were equipped with jacketed cell holders having temperature control within ± 0.1 °C. Spectrofluorometric titrations were done by adding increasing amounts of DNA directly to the cell containing the ZnL^{2+} solution, with both solutions under the same solvent conditions. In the experiments on the photochemical stability of ZnL^{2+} , the illumination was done using a tungsten lamp (60 W) placed at a fixed distance of 10 cm from the quartz cuvette (10 mm path length) containing the sample. The solvent polarity was expressed making use of the $E_T(30)$ scale (Dimroth–Reichardt ET parameter^[50]).

Acknowledgements

B.M. and A.B. acknowledge the European Research Council (ERC) for financial support in the framework of the Starting Grant (EnLight-277755). The financial support of “Obra Social La Caixa” is also gratefully acknowledged.

Keywords: density functional calculations • DNA recognition • intercalation • N,O ligands • photochemistry • photooxidation

- [1] a) P. A. Vigato, S. Tamburini, *Coordin. Chem. Rev.* **2004**, *248*, 1717–2128; b) P. Pfeiffer, E. Breith, E. Lubbe, T. Tsumaki, *Justus Liebigs Ann. Chem.* **1933**, *503*, 84–130.
- [2] G. Parkin, *Chem. Rev.* **2004**, *104*, 699–767.
- [3] a) S. J. Wezenberg, E. C. Escudero-Adan, J. Benet-Buchholz, A. W. Kleij, *Org. Lett.* **2008**, *10*, 3311–3314; b) M. E. Germain, M. J. Knapp, *J. Am. Chem. Soc.* **2008**, *130*, 5422–5423; c) M. Cano, L. Rodriguez, J. C. Lima, F. Pina, A. Dalla Cort, C. Pasquini, L. Schiaffino, *Inorg. Chem.* **2009**, *48*, 6229–6235; d) A. D. Cort, L. Mandolini, C. Pasquini, K. Rissanen, L. Russo, L. Schiaffino, *New J. Chem.* **2007**, *31*, 1633–1638.
- [4] K. Müllen, U. Scherf, *Organic Light Emitting Devices: Synthesis Properties and Application*, Wiley-VCH, Weinheim, **2006**.
- [5] a) N. Madhavan, C. W. Jones, M. Weck, *Accounts Chem. Res.* **2008**, *41*, 1153–1165b) D. J. Darensbourg, *Chem. Rev.* **2007**, *107*, 2388–2410; c) T. Katsuki, *Chem. Soc. Rev.* **2004**, *33*, 437–444; d) P. G. Cozzi, *Chem. Soc. Rev.* **2004**, *33*, 410–421.
- [6] a) S. J. Wezenberg, A. W. Kleij, *Angew. Chem.* **2008**, *120*, 2388–2399; *Angew. Chem. Int. Ed.* **2008**, *47*, 2354–2364; b) M. S. Masar, N. C. Gianneschi, C. G. Oliveri, C. L. Stern, S. T. Nguyen, C. A. Mirkin, *J. Am. Chem. Soc.* **2007**, *129*, 10149–10158; c) S. S. Sun, C. L. Stern, S. T. Nguyen, J. T. Hupp, *J. Am. Chem. Soc.* **2004**, *126*, 6314–6326.
- [7] N. H. Campbell, N. H. Abd Karim, G. N. Parkinson, M. Gunaratnam, V. Petrucci, A. K. Todd, R. Vilar, S. Neidle, *J. Med. Chem.* **2012**, *55*, 209–222.
- [8] T. Tekeste, H. Vahrenkamp, *Inorg. Chem.* **2006**, *45*, 10799–10806.
- [9] O. Alpturk, O. Rusin, S. O. Fakayode, W. H. Wang, J. O. Escobedo, I. M. Warner, W. E. Crowe, V. Kral, J. M. Pruet, R. M. Strongin, *P. Natl. Acad. Sci.* **2006**, *103*, 9756–9760.
- [10] G. Barone, A. Ruggirello, A. Silvestri, A. Terenzi, V. T. Liveri, *J. Inorg. Biochem.* **2010**, *104*, 765–773.
- [11] a) G. Barone, A. Terenzi, A. Lauria, A. M. Almerico, J. M. Leal, N. Busto, B. Garcia, *Coordin. Chem. Rev.* **2013**, *257*, 2848–2862; b) N. H. Abd Karim, O. Mendoza, A. Shivalingam, A. J. Thompson, S. Ghosh, M. K. Kuimova, R. Vilar, *RSC Adv.* **2014**, *4*, 3355–3363.
- [12] A. Silvestri, G. Barone, G. Ruisi, D. Anselmo, S. Riela, V. T. Liveri, *J. Inorg. Biochem.* **2007**, *101*, 841–848.
- [13] K. D. Mjos, C. Orvig, *Chem. Rev.* **2014**, DOI: 10.1021/cr400460s.
- [14] A. V. Klein, T. W. Hambley, *Chem. Rev.* **2009**, *109*, 4911–4920.
- [15] G. Barone, N. Gambino, A. Ruggirello, A. Silvestri, A. Terenzi, V. T. Liveri, *J. Inorg. Biochem.* **2009**, *103*, 731–737.
- [16] A. Terenzi, C. Ducani, L. Male, G. Barone, M. J. Hannon, *Dalton Trans.* **2013**, *42*, 11220–11226.
- [17] M. E. Germain, T. R. Vargo, B. A. McClure, J. J. Rack, P. G. Van Patten, M. Odoi, M. J. Knapp, *Inorg. Chem.* **2008**, *47*, 6203–6211.
- [18] N. J. Farrer, L. Salassa, P. J. Sadler, *Dalton Trans.* **2009**, 10690–10701; O. J. Stacey, S. J. A. Pope, *RSC Adv.* **2013**, *3*, 25550–25564.
- [19] a) K. E. Erkkila, D. T. Odom, J. K. Barton, *Chem. Rev.* **1999**, *99*, 2777–2795; b) A. J. McConnell, H. Song, J. K. Barton, *Inorg. Chem.* **2013**, *52*, 10131–10136.
- [20] A. Chantzis, T. Very, A. Monari, X. Assfeld, *J. Chem. Theory Comput.* **2012**, *8*, 1536–1541.
- [21] T. Etienne, T. Very, E. A. Perpete, A. Monari, X. Assfeld, *J. Phys. Chem. B* **2013**, *117*, 4973–4980.
- [22] J. Tomasi, B. Mennucci, R. Cammi, *Chem. Rev.* **2005**, *105*, 2999–3093.
- [23] a) A. Biancardi, T. Biver, A. Marini, B. Mennucci, F. Secco, *Phys. Chem. Chem. Phys.* **2011**, *13*, 12595–12602; b) A. Biancardi, T. Biver, F. Secco, B. Mennucci, *Phys. Chem. Chem. Phys.* **2013**, *15*, 4596–4603.
- [24] a) R. L. Martin, *J. Chem. Phys.* **2003**, *118*, 4775–4777; b) I. Mayer, *Chem. Phys. Lett.* **2007**, *437*, 284–286; c) A. V. Luzanov, A. A. Sukhorukov, V. A. Umanskii, *Theor. Exp. Chem.* **1976**, *10*, 354–361.
- [25] A. W. Lange, J. M. Herbert, *J. Am. Chem. Soc.* **2009**, *131*, 3913–3922.
- [26] A. Spinello, A. Terenzi, G. Barone, *J. Inorg. Biochem.* **2013**, *124*, 63–69.
- [27] C. Curutchet, A. Munoz-Losa, S. Monti, J. Kongsted, G. D. Scholes, B. Mennucci, *J. Chem. Theory Comput.* **2009**, *5*, 1838–1848.
- [28] S. Caprasecca, C. Curutchet, B. Mennucci, *J. Chem. Theory Comput.* **2012**, *8*, 4462–4473.
- [29] A. Chantzis, T. Very, C. Daniel, A. Monari, X. Assfeld, *Chem. Phys. Lett.* **2013**, *578*, 133–137.
- [30] T. Biver, A. De Biasi, F. Secco, M. Venturini, S. Yarmoluk, *Biophys. J.* **2005**, *89*, 374–383.
- [31] M. T. Record, C. F. Anderson, T. M. Lohman, *Q. Rev. Biophys.* **1978**, *11*, 103–178.
- [32] T. Biver, F. Secco, M. R. Tine, M. Venturini, A. Bencini, A. Bianchi, C. Giorgi, *J. Inorg. Biochem.* **2004**, *98*, 1531–1538.
- [33] J. B. Chaires, *Arch. Biochem. Biophys.* **2006**, *453*, 26–31.
- [34] C. Bazzicalupi, A. Bencini, A. Bianchi, T. Biver, A. Boggioni, S. Bonacchi, A. Danesi, C. Giorgi, P. Gratterri, A. M. Ingrain, F. Secco, C. Sissi, B. Valtancoli, M. Venturini, *Chem. Eur. J.* **2008**, *14*, 184–196.
- [35] Y. Zhao, N. E. Schultz, D. G. Truhlar, *J. Chem. Theory Comput.* **2006**, *2*, 364–382.
- [36] E. G. Hohenstein, S. T. Chill, C. D. Sherrill, *J. Chem. Theory Comput.* **2008**, *4*, 1996–2000.
- [37] S. F. Sousa, E. S. Carvalho, D. M. Ferreira, I. S. Tavares, P. A. Fernandes, M. J. Ramos, J. A. N. F. Gomes, *J. Comput. Chem.* **2009**, *30*, 2752–2763.
- [38] E. Cancès, B. Mennucci, J. Tomasi, *Journal Chem. Phys.* **1997**, *107*, 3032–3041.
- [39] B. Hess, C. Kutzner, D. van der Spoel, E. Lindahl, *J. Chem. Theory Comput.* **2008**, *4*, 435–447.

- [40] J. M. Wang, P. Cieplak, P. A. Kollman, *J. Comput. Chem.* **2000**, *21*, 1049–1074.
- [41] a) A. Perez, I. Marchan, D. Svozil, J. Sponer, T. E. Cheatham, C. A. Loughton, M. Orozco, *Biophys. J.* **2007**, *92*, 3817–3829; b) A. T. Guy, T. J. Piggot, S. Khalid, *Biophys. J.* **2012**, *103*, 1028–1036.
- [42] a) M. Svensson, S. Humbel, R. D. J. Froese, T. Matsubara, S. Sieber, K. Morokuma, *J. Phys. Chem.* **1996**, *100*, 19357–19363; b) T. Vreven, K. Morokuma, *J. Comput. Chem.* **2000**, *21*, 1419–1432.
- [43] a) U. C. Singh, P. A. Kollman, *J. Comput. Chem.* **1984**, *5*, 129–145; b) B. H. Besler, K. M. Merz, P. A. Kollman, *J. Comput. Chem.* **1990**, *11*, 431–439.
- [44] B. T. Thole, *Chem. Phys.* **1981**, *59*, 341–350.
- [45] P. T. van Duijnen, M. Swart, *J. Phys. Chem. A* **1998**, *102*, 2399–2407.
- [46] a) P. Slavicek, B. Winter, M. Faubel, S. E. Bradforth, P. Jungwirth, *J. Am. Chem. Soc.* **2009**, *131*, 6460–6467; b) K. C. Lau, C. Y. Ng, *Accounts Chem. Res.* **2006**, *39*, 823–829; c) D. M. Close, *J. Phys. Chem. A* **2011**, *115*, 2900–2912; d) T. B. Truong, *J. Phys. Chem.* **1980**, *84*, 964–970.
- [47] Gaussian 09, Revision H.11, M. J. Frisch, G. W. Trucks, H. B. Schlegel, G. E. Scuseria, M. A. Robb, J. R. Cheeseman, G. Scalmani, V. Barone, B. Men-
nucci, G. A. Petersson, H. Nakatsuji, M. Caricato, X. Li, H. P. Hratchian,
A. F. Izmaylov, J. Bloino, G. Zheng, J. L. Sonnenberg, M. Hada, M. Ehara,
K. Toyota, R. Fukuda, J. Hasegawa, M. Ishida, T. Nakajima, Y. Honda, O.
Kitao, H. Nakai, T. Vreven, J. Montgomery, J. A., J. E. Peralta, F. Ogliaro,
M. Bearpark, J. J. Heyd, E. Brothers, K. N. Kudin, V. N. Staroverov, R. Ko-
bayashi, J. Normand, K. R. Raghavachari, T. Nakajima, Y. Honda, O. Kitao,
H. Nakai, T. Vreven, J. Montgomery, J. A., J. E. Peralta, F. Ogliaro, M. Bear-
park, J. J. Heyd, E. Brothers, K. N. Kudin, V. N. Staroverov, R. Kobayashi, J.
Normand, K. Raghavachari, A. Rendell, J. C. Burant, S. S. Iyengar, J.
Tomasi, M. Cossi, N. Rega, J. M. Millam, M. Klene, J. E. Knox, J. B. Cross, V.
Bakken, C. Adamo, J. Jaramillo, R. Gomperts, R. E. Stratmann, O. Yazyev,
A. J. Austin, R. Cammi, C. Pomelli, J. W. Ochterski, R. L. Martin, K. Moro-
kuma, V. G. Zakrzewski, G. A. Voth, P. Salvador, J. J. Dannenberg, S. Dap-
prich, A. D. Daniels, Ö. Farkas, J. B. Foresman, J. V. Ortiz, J. Cioslowski,
D. J. Fox, Gaussian Inc., Wallingford CT, **2009**.
- [48] B. Garcia, J. M. Leal, R. Ruiz, T. Biver, F. Secco, M. Venturini, *J. Phys. Chem. B* **2010**, *114*, 8555–8564.
- [49] M. E. Reichmann, S. A. Rice, C. A. Thomas, P. Doty, *J. Am. Chem. Soc.* **1954**, *76*, 3047–3053.
- [50] C. Reichardt, *Angew. Chem.* **1965**, *77*, 30–40; *Angew. Chem. Int. Ed. Engl.* **1965**, *4*, 29–40.

Received: December 13, 2013

Published online on May 14, 2014